Heliyon 8 (2022) e09554

Contents lists available at ScienceDirect

Heliyon

journal homepage: www.cell.com/heliyon

Research article

Photoluminescent neodymium-doped ZnO nanocrystals prepared by laser ablation in solution for NIR-II fluorescence bioimaging

Natalie Tarasenka [a,*], Vladislav Kornev [a], Andrei Ramanenka [a], Ruibin Li [b], Nikolai Tarasenko [a]

[a] B. I. Stepanov Institute of Physics, National Academy of Sciences of Belarus, Minsk, 220072, Belarus
[b] State Key Laboratory of Radiation Medicine and Protection, School for Radiation Medicine & Interdisciplinary Sciences, Soochow University Suzhou, Jiangsu, 215123, China

ARTICLE INFO

Keywords:
Zinc oxide nanoparticles
Doped nanocrystals
Laser ablation in liquids
NIR-II photoluminescence

ABSTRACT

The work reports on the use of laser ablation and post-ablation irradiation techniques for the preparation Nd^{3+} doped ZnO nanoparticles (NPs). The focus has been made on photoluminescence of Nd-doped ZnO NPs in the second near infrared (NIR-II) spectral window (1000–1700 nm) of the biological transparency. Morphology, phase composition and optical properties of the synthesized NPs were studied by absorption and photoluminescence spectroscopy, X-Ray diffraction (XRD) and transmission (TEM) electron microscopy. Near-infrared luminescence of Nd^{3+} doped ZnO nanocrystals in the region of 1000–1400 nm was detected both upon excitation from the ground state (800 nm) and upon UV excitation. The latter proves the incorporation of the Nd^{3+} into ZnO lattice as photoluminescence occurs through the transfer of excitation energy from the ZnO matrix to the Nd^{3+} ion. The possibility of control over the luminescence properties by a variation of solvent composition and by additional laser irradiation was demonstrated.

1. Introduction

In the past decade, rare-earths activated nanoparticles (NPs) due to their prominent photoluminescent properties, electronic and energy level structure have attracted much attention for a range of practical applications, including bioimaging and labeling, theranostics, fabrication of optoelectronic devices, electronic displays, LEDs, etc. [1, 2, 3, 4, 5]. Upon lanthanide ions incorporation into a transition metal oxide matrix, novel luminescent materials can be produced having high photostability and quantum yield, long emission lifetime, narrow line widths and large Stokes shifts. Nevertheless, preparation of nanosized lanthanide-doped NPs is still challenging [3]. At present, for the synthesis of NPs various physical, chemical and physico-chemical techniques are used. However, preparation of non-agglomerated and pure (surfactant-free) NPs with the required morphologies and high crystallinity suitable for their successful practical applications has still not been achieved and is under development. Due to the large ionic radius mismatch between rare-earth and transition metal ions, creation of luminescent rare earth centers in a host metal oxide NP by chemical means remains a problem. Moreover, conventional wet-chemistry approaches often require use of organic solvents or surfactant addition for NP size control that may result in the production of toxic by-products thus hindering biomedical applications of the resulting NPs. Therefore, development of new and cost-efficient technologies to produce high-quality nanosized lanthanide-doped particles with improved luminescence properties is highly anticipated. Among the different synthesis methods, liquid-assisted laser ablation has now established as an effective tool for fabrication of nanomaterials with sizes, shapes, composition and structure varying in a broad range [6, 7]. The pulsed laser ablation in liquids (PLAL) enables a simple production process with the possibility of control over their morphology and inner structure upon the variation of laser parameters, as well as capable of composite nanostructures synthesis by combination of ablation and laser-induced modification processes [8, 9, 10, 11]. Concerning the biomedical applications, the beneficial property of laser ablation in liquids (LAL) is a high colloidal stability of laser-produced NPs (usually up to several months) without a need in additional stabilizers. Also, the PLAL technique allows excluding the use of toxic chemicals and avoiding the formation of by-products, thus providing a clean, eco-friendly and bio-safe approach suitable for biomedical applications. Specifically for doped NPs formation, the creation of high temperature and pressure conditions in laser ablation process may be a valuable feature as that may promote the formation of doped NPs providing an increase of the inclusion of dopant atoms under the non-equilibrium conditions.

* Corresponding author.
E-mail address: natalie.tarasenka@ifanbel.bas-net.by (N. Tarasenka).

https://doi.org/10.1016/j.heliyon.2022.e09554
Received 19 April 2022; Received in revised form 22 May 2022; Accepted 24 May 2022

In this work, we developed a method for fabrication of Nd-doped zinc oxide NPs based on double-pulse laser ablation of Zn target in neodymium nitrate solution combined with a post-ablation irradiation of the formed colloid that allowed varying the NPs characteristics and properties. The main focus of the work was on the photoluminescence of the prepared colloidal NPs in the NIR-II spectral biological transparency window in dependence on the experimental conditions that was performed to test their applicability as potential photoluminescent components for bioimaging.

Zinc oxide is a non-toxic semiconducting material with a wide bandgap, which can be used as a suitable matrix. To date, preparation of the doped ZnO NPs has received much attention [12, 13], but most of the works is aimed to fabricate NPs exhibiting luminescence in the visible spectral region. It is expected that ZnO nanocrystals doped with lanthanide ions will form a photoluminescent material in the near infrared region of 800–1400 nm (NIR) [14, 15]. In particular, ZnO nanocrystals doped with neodymium ions, which have several important luminescent bands in the NIR region, including the transitions $^4F_{3/2} \rightarrow {}^4I_{9/2}$ (at ~ 900 nm), $^4F_{3/2} \rightarrow {}^4I_{11/2}$ (1060 nm) and $^4F_{3/2} \rightarrow {}^4I_{13/2}$ (1340 nm) [16], are of interest for applications as luminescent biomarkers, as maximal light transmission of biological tissues is reported to be in the 850–1100 nm region [17]. Among the other applications, Nd-doped ZnO NPs have shown promising photocatalytic properties for water purification [18, 19].

The main strategy for the improvement of luminescent properties is to increase the concentration of the dopant in the zinc oxide matrix, that requires further optimization of the conditions for the particles synthesis. The major problems hindering the achievement of high dopant concentrations in oxide matrices are the low solubility of the impurity due to the significant difference in the impurity and matrix atoms radii, the formation of defects in the matrix, as well as segregation of secondary phases, formation of defect complexes and their clusters with an increase of the impurity concentration in the lattice. The solubility of dopant can be increased by using non-equilibrium growth methods, that suppress the release of the secondary phases [20]. Therefore, application of laser-induced plasma methods, that are utilizing non-equilibrium conditions of NPs formation, may enhance the introduction of dopant impurities into the particles structure. In general, the doping process is determined by the conditions of the nanocrystals growth, that in the case of PLAL synthesis depend on the conditions in the formed plasma plume and on the liquid medium where the particles are formed (from oxygen-saturated to a medium with a high zinc content).

The particles formed by laser ablation in an aqueous solution of neodymium nitrate may contain internal defects such as zinc (V_{Zn}) and oxygen (V_O) vacancies, interstitial oxygen (O_i) and zinc (Zn_i) atoms, as well as anti-structural defects Zn_O and O_{Zn}, as well as their complexes, which also can decrease the intensity of the luminescence of the Nd^{3+} ion. Therefore, the strategies to increase the luminescence intensity of the doped ZnO NPs were analyzed based on the study of solvent selection and additional laser irradiation impact on the particles morphology, crystallinity and the optical properties of the dopant in the ZnO matrix.

2. Experimental section

For the ZnO:Nd^{3+} colloidal NPs preparation, the setup presented in Figure 1a was used. The detailed description of the experimental conditions has been reported previously (see, for example [21]). Briefly, laser ablation synthesis was performed by focusing the radiation of a nanosecond-pulsed Nd^{3+}:YAG laser (LOTIS TII, LS 2134D, Belarus) on the surface of a pure zinc plate by a 75 mm lens. The laser was operating in a double-pulse mode providing a sequence of two delayed laser pulses with the interpulse delay of 10 μs. The fundamental harmonic of the laser (wavelength 1064 nm) was used for the ablation with the following parameters: laser pulse energy 80 mJ/pulse, pulse duration 10 ns, repetition rate 10 Hz. As a neodymium ion source, 0.01 M $Nd(NO_3)_3{\cdot}6H_2O$ aqueous or ethanolic solutions were used to fill in the cuvette, where the Zn target was inserted during the ablation process. The power density of laser radiation on the target surface was estimated to be $5.5{\cdot}10^8$ W/cm^2.

Laser action on the target results in the formation of plasma near the surface of a target (Figure 1b). After its collapse, NPs formation occurs in result of the condensation of atoms and small clusters formed in the ablation plasma plume. At this stage, an interaction with the components of the liquid that contains dopant ions is possible. Besides, during the formation of NPs in the plasma phase, the nuclei of the growing particles are negatively charged [22]; therefore, the growth of nuclei occurs due to the attraction of ions. As a result, additional laser irradiation of the NPs can lead to the particles melting and structural rearrangements that may result in the increased incorporation of dopant into the NPs structure.

At the second stage, the prepared colloid was subjected to the additional laser modification. This method is based on the irradiation of as-prepared colloidal NPs with the unfocused laser beam. The scheme of this process is presented in Figure 1c. In the performed experiments, the second harmonic of the nanosecond pulsed Nd^{3+}:YAG laser (pulse duration 10 ns, repetition rate 10 Hz, wavelength 532 nm, laser fluence 0.32 J/cm^2) was used. For the modification, a portion (10 mL) of the prepared colloid was placed in a glass cuvette and irradiated for 30 min.

The formed NPs were characterized by means of transmission electron microscopy (TEM, LEO 906E), X-Ray diffraction, absorption and photoluminescence spectroscopy. The size and morphology of the

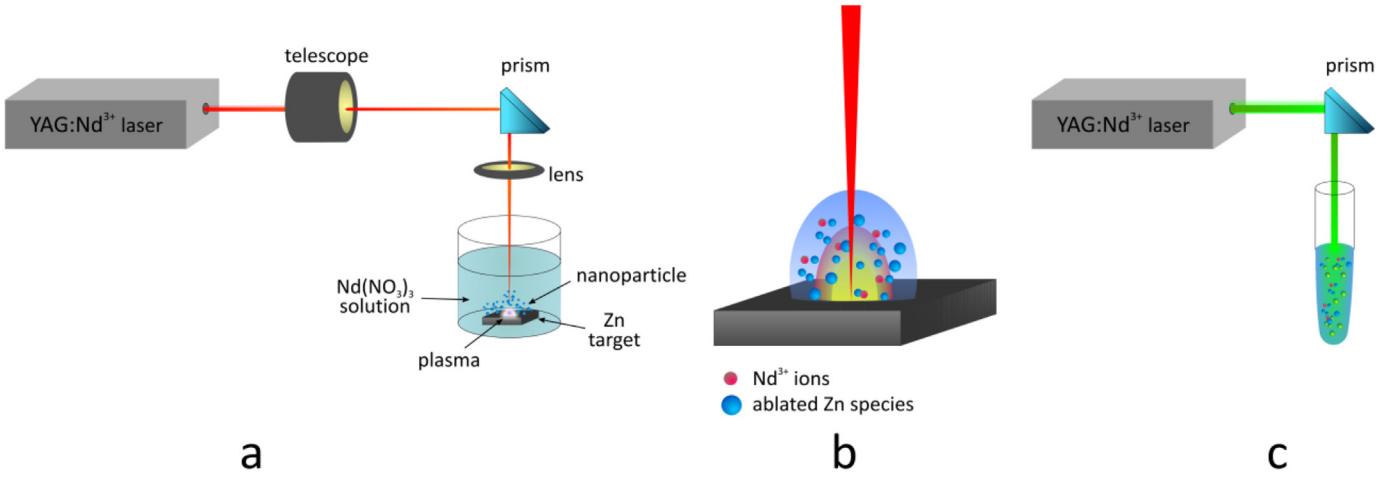

Figure 1. Schematic diagrams of (a) LAL process to prepare doped zinc oxide NPs as a first stage, which is based on the formation of plasma near the target surface (b); and (c) laser-assisted modification of as-prepared NPs as a second stage.

particles were elucidated from the TEM results. The samples for the TEM investigations were prepared by drop-casting of the formed colloid onto a carbon-coated copper grid with further drying at room temperature. The size distribution of the particles was evaluated from the analysis of more than 100 particles in each sample.

The crystalline phases of the samples were determined by powder X-Ray diffraction technique using a modified D8-Advance X-ray diffractometer (Bruker, Germany) in the mode of recording X-ray diffraction patterns by points at T ≈ 300 K in the angle range (2Θ) from 30 to 60°. To perform X-ray diffraction studies, the investigated colloidal solution was deposited onto the glass substrate and dried at room temperature. The relative positions of the peaks were determined in accordance with the JCPDS database. The phase was considered identified when three to five reflections of the most intense lines coincided with the table values.

For the analysis of the optical properties, two techniques were used: absorption and photoluminescent spectroscopy. The measurement of the absorption spectra was performed using a Cary-500 Scan (USA) spectrophotometer operating in the wavelength range from 200 to 1300 nm. The colloid was placed in a 1 cm quartz cuvette.

The photoluminescence (PL) spectra of the prepared colloids were measured at room temperature using a Fluorolog-3 spectrofluorometer (HORIBA Scientific, USA) equipped with Peltier-cooled silicon Syncerity CCD-detector (visible range) and liquid-nitrogen cooled InGaAs Symphony II CCD-detector (NIR range). NIR PL excitation spectra were measured with liquid-nitrogen cooled R5509-74 PMT-detector (Hamamatsu, Japan). All the registered spectra were measured in front-face geometry and were corrected for the spectral sensitivity of the spectrofluorometer.

3. Results and discussion

3.1. Morphology studies

As expected, the liquid environment has a strong influence on the structural and morphological parameters of the NPs prepared by laser ablation. As it follows from the Figure 2, the particles average size reduced and size distribution narrowed for the sample prepared by laser ablation in $Nd(NO_3)_3$ solution (Figure 2b) as compared to the pure aqueous colloid (Figure 2a). Indeed, the diameters of the particles formed in distilled water were mainly distributed in the range 1–50 nm (Figure 2d), while in the salt solution the particles were distributed in the range 1–10 nm (Figure 2e).

The particles formed by laser ablation in Nd nitrate solution were found to be round-shaped and uniform. The average diameter of the particles is lower in the sample prepared by laser ablation in a salt solution: for the particles prepared in water it was found to be 14 nm while in $Nd(NO_3)_3$ it reduces down to 4 nm. In addition, particles appear to be less aggregated in the salt solution while non-spherical structures found in the sample prepared in pure water were not observed in the case of synthesis in the salt solution.

The reduction of the particles diameter can be attributed to the mechanisms of nanoparticle formation in laser-induced plasma. It is known that pulsed laser action on a bulk target placed in a liquid results in the formation of a plasma plume near the target surface (Figure 1b). During laser ablation, the formation of particle nuclei begins in the plasma medium within the first few hundred of nanoseconds. In the next microseconds, NPs can undergo structural rearrangements in the cavitation bubble and are finally released into the surrounding liquid [22].

The change in the charge on a particle surface by the addition of electrolytes during the ablation process can serve as a tool for adjustment of the colloids stability and NPs size, since the surface charge can also arise in result of the adsorption of charged particles present in the solution. In this case, the processes of charging and aggregation of particles will depend on the pH, ionic strength and nature of the ions present in the solution [23]. Although typically an increase in the solution ionic strength reduces the colloid stability, the adsorption of ions at a target/liquid interface can promote the transfer of ions charge to the NPs surface, leading to the repulsive interactions between growing NPs and their subsequent stabilization [24]. The authors in [24] pointed out that the ions in the colloidal solution also induce the confinement effect on the NP growth during PLAL thus resulting in the NPs average size reduction and size distribution narrowing.

After laser irradiation, the particles diameters are distributed within the range 1–14 nm while the average size reduces up to 2.3 nm (Figure 2f). The fragmentation of the particles may be a consequence of NPs heating by nanosecond laser pulses. However, the formation of larger aggregates is also observed after laser treatment (Figure 2c).

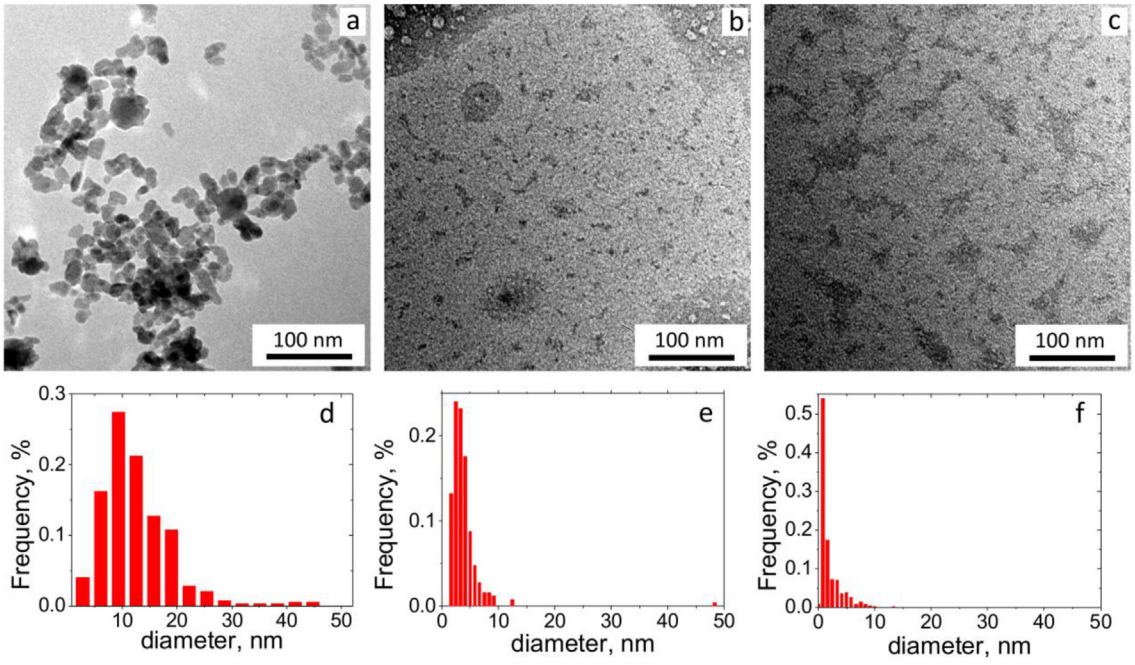

Figure 2. TEM images of the NPs prepared by laser ablation of Zn target in water (a) and in $Nd(NO_3)_3$ solution before (b) and after (c) additional laser irradiation. Figures (d)–(f) show the corresponding size distributions for the NPs in distilled water (d) and $Nd(NO_3)_3$ solution before (e) and after (f) laser modification

3.2. Structural analysis

The phase composition of laser-synthesized NPs was analyzed using X-Ray diffraction technique. Figure 3 shows the XRD pattern of the ZnO:Nd sample before and after laser irradiation along with the sample prepared by laser ablation in distilled water presented for comparison. The latter sample shows the features typical to the distorted nanostructures: broad peaks with low intensity that can be attributed to the hexagonal ZnO phase. The major peaks in the sample prepared in water are observed at $2\theta = 31.8°$, 34.4°, 36.1°, 47.6°, 56.5°, which correspond well to the (100), (002), (101), (102), (110), planes of the crystalline hexagonal wurtzite ZnO phase having the space group P63mc (JCPDS 36−1451).

For the ZnO NPs obtained by laser ablation in a neodymium nitrate solution before and after irradiation with the second harmonic of the Nd:YAG laser (532 nm), a number of additional peaks were found. Namely, the presence of excess neodymium nitrate hexahydrate was observed in both cases. Besides, the phase of neodymium oxynitrate $NdONO_3$ having orthorhombic structure appears that can be due to the decomposition of the $Nd(NO_3)_3$ present in the solution. The intensity of the peaks attributable to this phase significantly decreases after additional laser treatment due to its decomposition under heating by intense laser pulses. In addition, the diffraction peaks attributable to the reflections of the hexagonal and cubic neodymium oxide were also observed.

The intensity of these phases is also susceptible to the additional laser irradiation as the intensity of cubic neodymium oxide peaks sufficiently decreases after the laser treatment while the hexagonal oxide phase peaks were not found. These results indicate that laser irradiation induces decomposition of the impurity phases thus causing the purification of the sample.

As for the Zn-containing phases, the presence of the metallic Zn was observed that was concluded from the observation of (100) and (101) reflections of the zinc phase with hexagonal structure. The peaks corresponding to the Zn phase are rather intensive and narrow and thus it can be assumed that they come from the large particles obtained through the ejection mechanism from the target.

The peaks corresponding to the hexagonal ZnO phase were observed in all the samples. However, synthesis in the $Nd(NO_3)_3$ solution results in the peaks shift and the intensities re-distribution as can be seen in Figure 3: the (101) peak significantly broadens and drops in intensity in the Nd-containing samples while the (002) and (100) peaks intensity increases. Typically, redistribution of the ZnO peaks intensities indicates the distortion of its lattice that may be caused by the incorporation of dopant atoms. Wurtzite has an open structure with interstitials, thus the rare earth atoms may occupy Zn^{2+} site or Zn interstitial position thus replacing or displacing Zn^{2+} ions in the crystalline structure [25]. Due to the Nd^{3+} ion larger ionic radius (0.94 Å) compared to the Zn^{2+} ion (0.74 Å) [25] doping with neodymium introduces significant strain into the ZnO lattice and increases the amount of structural defects, such as oxygen vacancies. In the both samples obtained in $Nd(NO_3)_3$, the (002) and (101) diffraction peaks get shifted towards the lower angle that can be caused by the expansion of the unit cell along c and a-axes because of the large ionic radius mismatch. Such a behavior is related to the substitution of Zn^{2+} by Nd^{3+} ions and therefore confirms the ZnO NPs doping.

3.3. UV-Vis absorption

The UV-Vis spectroscopy was used to clarify the absorption properties of the prepared colloids of Nd^{3+} doped ZnO NPs in the wavelength range 200–1300 nm. The absorption spectra of NPs obtained by laser ablation of a zinc target in a neodymium nitrate aqueous solution before and after laser-induced modification are shown in Figure 4a. It can be seen from the absorption spectra that doped ZnO has a sufficiently high transmittance in the visible and near IR regions. In addition, the spectra of NPs in solution exhibit a rather sharp absorption edge at about 375 nm, on the edge of the fundamental absorption band of zinc oxide. Thus, the absorption spectra prove the formation of the colloid containing zinc oxide NPs.

The bandgap values E_g can be obtained from the spectra analysis using the Tauc method (Figure 4b). As ZnO is known to be a direct-bandgap semiconductor, plotting the absorption spectrum in the $(\alpha h\nu)^2$ *vs* $h\nu$ coordinates allows to find the optical bandgap. The corresponding results are shown in Figure 4b. It is noteworthy that the optical bandgap of the ZnO:Nd NPs is slightly larger than that of the sample prepared in water in similar conditions: 3.33 eV vs 3.30 eV. This slight bandgap increase can be explained by Burstein-Moss effect [26] due to zinc oxide doping or by NPs size reduction. From the analysis of the NPs absorption spectra near the edge of the ZnO fundamental absorption band (about 375 nm), it can be concluded that the additional laser irradiation does not significantly change the bandgap of the sample but can improve the quality of the crystal lattice, exhibiting a sharper absorption edge near 375 nm. Besides the absorption band of ZnO, several additional absorption peaks were found in the spectra, that can be attributed to the

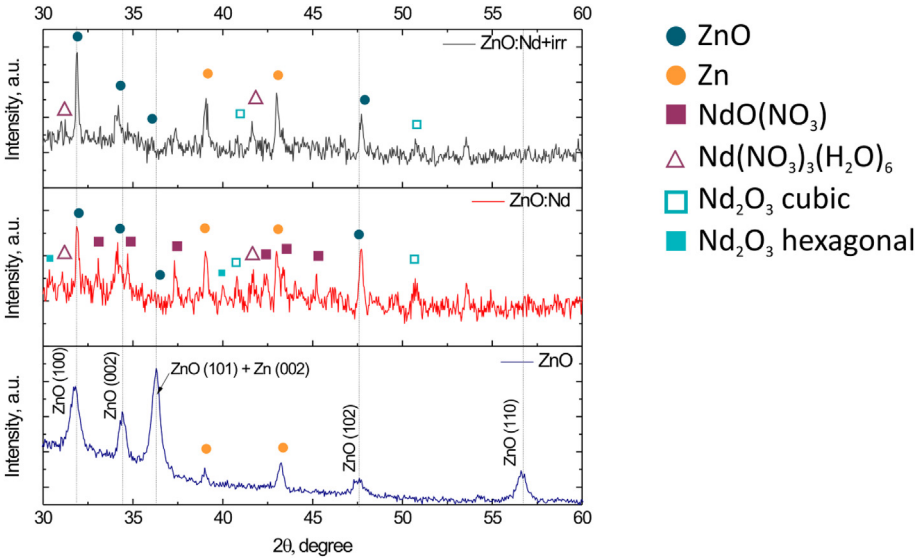

Figure 3. X-ray diffraction patterns of ZnO NPs obtained by laser ablation in water and in neodymium nitrate solution before and after irradiation of the colloid with the second harmonic of the Nd:YAG laser (532 nm).

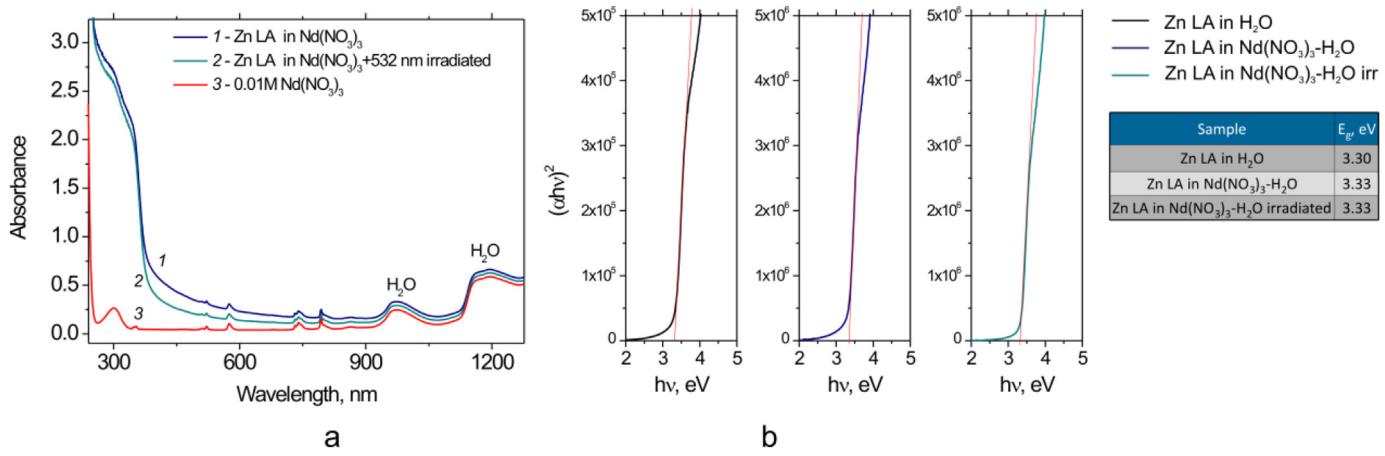

Figure 4. Absorption spectra (a) and $(\alpha h\nu)^2$ *vs* $h\nu$ (b) dependences for the NPs obtained by laser ablation of a zinc target in a neodymium nitrate solution in water before and after 532 nm laser irradiation. The inset table shows the corresponding bandgap values for the samples.

transitions of neodymium ion from the $^4I_{9/2}$ ground state to the following excited levels: $^2K_{13/2}+^4G_{9/2}$, (at 512 nm), $^4I_{9/2}\rightarrow{}^4G_{7/2}+^4G_{9/2}+^2K_{13/2}$ (522 nm), $^4I_{9/2}\rightarrow{}^4G_{5/2}+^2G_{7/2}$ (575 nm), $^4I_{9/2}\rightarrow{}^4F_{7/2}+^4S_{3/2}$ (740 nm) and $^4I_{9/2}\rightarrow{}^4F_{5/2}+^2H_{9/2}$ (794 nm) (Figure 4a) [27, 28].

3.4. Photoluminescence analysis of the Nd^{3+} incorporation into ZnO nanoparticles

To further study the incorporation of the Nd^{3+} into the structure of the prepared NPs the luminescence measurements of the colloids were carried out in the visible in near-infrared regions (Figure 5). The prepared samples emit the luminescence in both regions under UV excitation. ZnO:Nd colloids exhibit luminescence in the entire visible region, showing the features typical to the distorted ZnO nanostructures: namely, two intensive broad bands centered at around 430 nm and 600 nm are registered (Figure 5a). The broad emission in ZnO nanostructures is commonly observed and is typically ascribed to the defect-induced transitions such as oxygen and zinc interstitials, their vacancies and antisites [29]. The formation of defects is typical to the particles prepared by laser ablation in liquids; however, additional defect levels may be formed upon the incorporation of neodymium atoms into the zinc oxide structure that can trap free carriers resulting in a higher visible emission. It is noteworthy that several spectral dips are observed at around 522 nm, 575 nm and 740 nm that correspond well to the absorption of Nd^{3+} ions (see Figure 4a) and thus can be attributed to the re-absorption of the emitted light by Nd^{3+} ions.

Internal defects of the oxide matrix, such as zinc (V_{Zn}) and oxygen (V_O) vacancies, interstitial oxygen (O_i) and zinc (Zn_i) atoms, as well as Zn_O and O_{Zn} antisite defects create defect levels near the conduction and valence bands. Thus, the broad luminescence band in the visible region of the spectrum is the result of superposition of radiation from the different levels emitting simultaneously. According to [30], where the energy levels between different defect centers were calculated, the blue emission can be associated with the transitions from the interstitial zinc level to the valence band. The corresponding transition energy is 2.9 eV (about 425 nm), which corresponds to blue emission from ZnO. Zn_i typically acts as a shallow donor and the corresponding defect level is situated slightly below the conduction band-edge. According to a number of works, the blue emission can also be associated with an electronic transition from the donor energy level of the interstitial zinc atom to the acceptor energy level of zinc vacancy [31].

Green luminescence with transition energies in the 2.4–2.5 eV range is the most studied defect emission in ZnO and can be attributed to the several sources: V_{Zn}, V_O, O_i, Zn_i and V_OZn_i clusters [30]. The yellow emission band, observed in the range of about 2.2 eV, is associated with interstitial oxygen atoms or hydroxyl groups bounded to the surface of ZnO NPs [32]. Orange, orange-red, and red luminescence bands are also observed in ZnO, and they can be attributed to the transitions associated with interstitial oxygen atoms [33], complexes of zinc vacancies [34] and interstitial zinc atoms [35], respectively.

Thus, the appearance of luminescence in the visible region can be attributed to the transitions related to the defects created in the ZnO structure. At low concentrations, internal defects can increase the probability of transitions of rare-earth ions incorporated into the matrix and thus increase the luminescence intensity of rare-earth ions incorporated into the ZnO matrix. However, due to the fact that during the formation of internal defects, such as oxygen vacancies, the crystallinity of the samples is disturbed, an increase in the concentration of intrinsic crystal defects more commonly leads to the quenching of luminescence associated with the transitions of rare-earth ions [36].

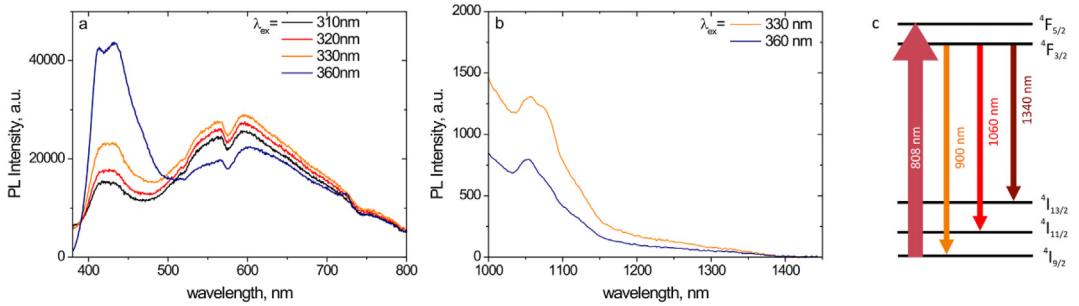

Figure 5. Photoluminescence spectra of ZnO NPs colloidal solutions prepared by laser ablation of metallic zinc in neodymium nitrate aqueous solution in the visible (a) and near-IR regions (b) at different excitation wavelengths. Figure c illustrates a simplified diagram of the energy levels of the Nd^{3+} ion, showing the main absorption and emission transitions in the near infrared region.

The spectral features in the visible region do not significantly change upon the variation of the excitation wavelength in the 310–360 nm region while the positions of the bands remain mainly unchanged. Still, with the increase of the excitation wavelength the intensity of the short-wavelength emission increases while the long-wavelength defect-related band shows a complex behavior with overall decrease in intensity.

The room-temperature PL spectra of the ZnO:Nd sample in water in the NIR region obtained for the 330 and 360 nm excitation are shown in Figure 5b. The spectra are dominated by a broad asymmetric band in the 1040–1080 nm region that can be attributed to the emission of Nd^{3+} ions from $^4F_{3/2}$ excited level to $^4I_{11/2}$ ground state (see Figure 5c). The observation of Nd^{3+} emission bands under UV excitation, where Nd^{3+} does not have characteristic absorption bands, gives a direct evidence of Nd^{3+} incorporation into the ZnO matrix: in this case the emission occurs through ZnO excitation with the subsequent excitation energy transfer from the ZnO host to the introduced neodymium ion. Such indirect excitation has been previously reported for the Nd^{3+} incorporated into ZnO [37, 38] and TiO_2 [39,40] matrices that results in a more complex emission spectrum than in the case of direct excitation [38].

The NIR PL band consists of several overlapping counterparts mainly at 1047 and 1075 nm that indicates that Nd^{3+} is present in several luminescent sites in the prepared nanostructures. The position and shape of the bands does not significantly change upon the increase of the excitation wavelength from 330 to 360 nm but the intensity of the NIR PL band decreases that is consistent with the overall decrease of the visible long wavelength defect-related emission upon the increase of the excitation wavelength (Figure 5a).

For further modification and control over the Nd^{3+} incorporation and emission two strategies were applied: additional laser modification and variation of the solvent used for laser ablation. The spectra of the ZnO:Nd sample in water before and after additional 532-nm laser treatment are shown in Figure 6. The spectrum of the solvent (0.01 M Neodymium III Nitrate Hexahydrate (aq)) is shown for comparison. It is noteworthy that in the latter case no detectable PL emission was observed. On the contrary, in the prepared samples both before and after laser irradiation the colloids demonstrate the emission band at around 1060 nm that again confirms excitation energy transfer from ZnO matrix and thus the incorporation of Nd^{3+} into the ZnO lattice. The peak is, however, broad, asymmetric and non-uniform that can be attributed to the formation of several luminescent sites by Nd ions. In the spectra of both as-prepared and irradiated samples the characteristic features are the same: two components can be highlighted: at around 1047 and 1075 nm. After laser irradiation, these features blue-shift and the overall intensity of the PL band increases that can be indicative of the increase of the Nd incorporation in result of the laser-induced modification.

Laser action on the colloidal solution results in the absorption of the laser radiation with further relaxation of the absorbed energy that in the case of nanosecond laser pulses results in heating of the particles. In case if incident energy is high enough, the particles can be melted and rapidly re-crystallize. At this point, the interaction of the heated particle is possible with the surrounding liquid that still contains the Nd^{3+} ions that are adsorbed at the surface and stabilize the particles. Therefore, laser-induced modification may further increase the concentration of the dopant in the ZnO NPs structure through the processes of laser-induced heating of the NP in dopant-containing colloid.

To further study the formed sites, the PL excitation spectra were analyzed, the results are presented in Figure 7. The spectra were recorded for the 1075 nm emission line. Overall, three bands were detected: at around 521 and 576 nm, that correspond well to the absorption bands of Nd^{3+} ion, and a broad intensive band at around 300–400 nm that is dominating the spectrum.

The latter can be attributed to the excitation of the ZnO lattice as it corresponds well to the ZnO NPs exciton absorption (see Figure 4). It is noteworthy that in the spectra of neodymium nitrate solution, shown in Figure 7 for comparison, the bands at around 524 and 576 nm were also observed, though differing in shape, whereas in the UV region a low-intensity symmetric band was observed that is also in agreement with the absorption spectroscopy observations. The Nd^{3+} peaks in the ZnO matrix are slightly red-shifted with respect to those in $Nd(NO_3)_3$ solution possibly due to the strong crystal field affecting the Nd^{3+} in the ZnO matrix. These results additionally prove the incorporation of Nd^{3+} into the ZnO lattice and excitation energy transfer from the excited ZnO nanocrystals to the Nd^{3+} ions resulting to the emission of the latter.

3.5. Study of the effect of liquid composition on the formation of neodymium-doped ZnO nanoparticles

Determination of the optical properties and structural characteristics dependence on the synthesis conditions makes it possible to optimize the process of NPs production having given properties. Among the experimental parameters affecting the physicochemical processes of NP formation, one of the crucial ones is the composition of a liquid medium where the target is ablated. The thermophysical properties of a liquid determine the cooling processes of NPs formed as a result of a plasma plume expansion and collapse that subsequently have an effect on the morphology, size, and phase composition of particles. In particular,

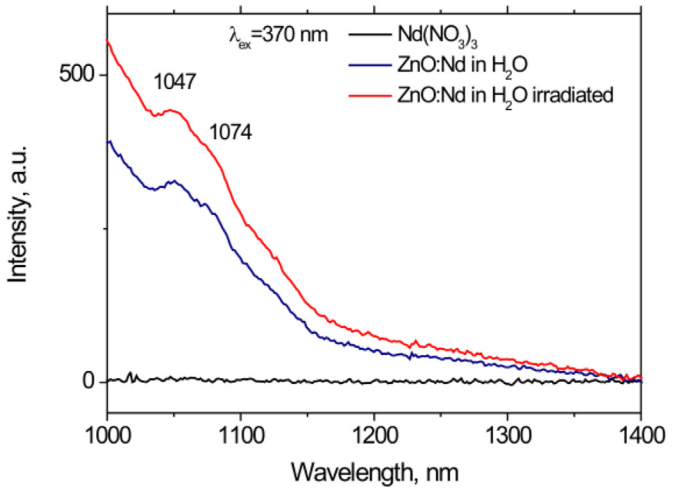

Figure 6. Emission spectra of ZnO: Nd^{3+} NPs in an aqueous solution before and after laser modification under the 370 nm excitation; the spectrum of the $Nd(NO_3)_3$ aqueous solution is shown for comparison.

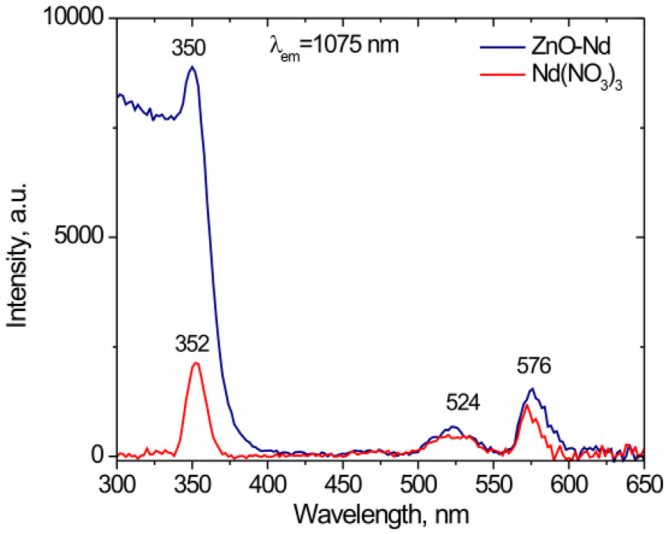

Figure 7. NIR PL excitation spectra of ZnO:Nd^{3+} NPs in an aqueous solution and $Nd(NO_3)_3$ in distilled water.

different cooling rates of particles in different liquids makes it possible to vary the defect structure, while a cooling time shortening allows creating non-equilibrium conditions that contribute to an increase in the concentration of introduced impurities and the production of metastable phases. Different density and viscosity of a liquid media can lead to a change in the pressure in the plasma plume, as well as vary the intensity of shock waves generated during ablation, which, in turn, can affect the size and morphology of NPs. Particle size distribution is another important parameter that depends on the composition of the solvent, in particular, in a synthesis in polar solvents containing ionic additives that determine the NPs surface charge.

Finally, the chemical properties and polarity of solvents determine the chemical and phase composition of the resulting NPs due to the reactions of ablated target material with solvent molecules both inside the plasma and at its boundary, and through the liquid reactions with the surface of formed particles, determining their structure (core-shell, oxide particles).

For the determination of the liquid impact on the luminescence properties of NPs, the synthesis of zinc oxide NPs was carried out in a solution of neodymium nitrate in two different liquids: water and ethanol. The choice of solvents is explained by the good solubility of neodymium nitrate in both cases as well as by difference in their properties, such as chemical composition, heat capacity, thermal conductivity, density, viscosity, polarity, etc. The experiments were done by focusing the beam of the fundamental harmonic of the Nd:YAG laser on a Zn target surface immersed in a 0.01 M solution of $Nd(NO_3)_3{\cdot}6H_2O$ in water or ethanol. The results of the optical properties study of NPs obtained in the aqueous and alcohol solutions of neodymium nitrate are shown in Figures 8, 9, and 10. The studies were carried out by optical absorption and luminescence spectroscopy.

As can be seen from the absorption spectra shown in Figure 8, colloidal solutions obtained in both solvents are characterized by an intense absorption band in the region of 200–450 nm, typical to the ZnO nanostructures exciton absorption, that may indicate the formation ZnO NPs in both cases. As can be seen, the intensity of the exciton band is much higher in water than in ethanol that may signify of more efficient ablation of zinc in water compared to ethanol.

Additional laser irradiation leads to a decrease in the intensity of absorption bands. In addition to the exciton absorption band of ZnO, the spectra also exhibit peaks at 521 nm, 578 nm, and 794 nm, which are characteristic absorption bands of the Nd^{3+} ion.

It was found that the composition of a liquid in which laser ablation occurs also affects the luminescence properties of the resulting NPs. As

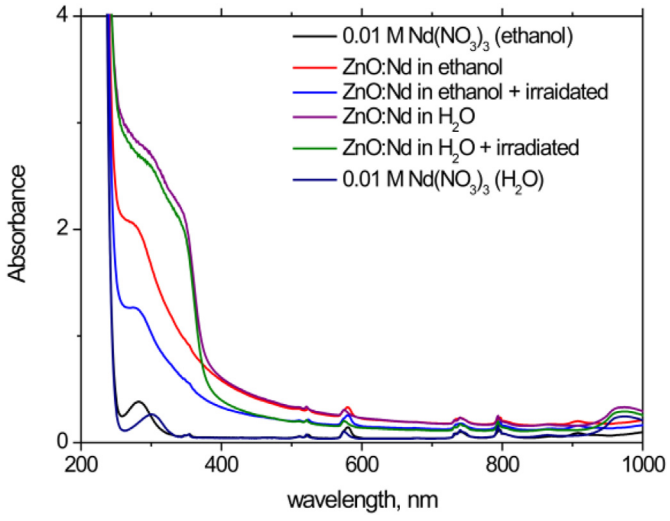

Figure 8. Absorption spectra of the colloids obtained by laser ablation of zinc in the aqueous and ethanol solutions of $Nd(NO_3)_3$.

shown in the previous section and in Figure 9, the ZnO:Nd colloid prepared in water exhibits luminescence in the entire visible region, which consists of two bands with maxima at about 420 and 600 nm, which is typical of defect-containing zinc oxide nanostructures. However, in the case of particles obtained in ethanol, no long-wavelength defective luminescence band is observed (Figure 9) that can be indicative of different defect sites created in the samples prepared in water and ethanol.

The luminescence spectra recorded in the IR range are shown in Figure 10. Figures 10 (a)–(d) demonstrate the differences in the PL emission spectra for the samples in water and ethanol at a selected excitation wavelength. The spectra of the initial solutions of Nd salt are presented for comparison. As can be seen from the presented spectra, excitation at wavelengths in the UV range leads to the appearance of emission in the 1050–1080 nm range, associated with the $^4F_{3/2} \rightarrow {}^4I_{11/2}$ transition of the Nd^{3+} ions [37]. Under the excitation in the UV region (330 and 360 nm), the intensity of the above mentioned PL band is higher in the prepared colloidal ZnO:Nd solutions both in water and in ethanol than in the spectra of the initial solvents.

Under the UV excitation, this band is asymmetric and broad on the contrary to the solvents luminescence, consisting of two major parts at around 1057 and 1075 nm, which indicate the presence of several Nd^{3+} emission centers in the solution. On the contrary, in the spectra of the initial solutions of neodymium nitrate in water and ethanol, the weak luminescence band appears under UV-excitation that is symmetric and narrow, with a maximum at 1054 nm for both solutions. Thus, the feature in the colloids at 1057 nm most probably is attributable to the excess of the Nd^{3+} ions in the solution while the long-wavelength band is associated with the incorporation of Nd^{3+} into the ZnO structure. This conclusion is supported by the lower intensity of the 1075 nm band in the PL spectra of ZnO:Nd in ethanol that corresponds well to the lower intensity of the exciton absorption in this colloid due to the lower ablation efficiency.

The luminescence spectra recorded at 360 nm excitation show similar behavior as at 330 nm: the luminescence of the ZnO:Nd colloid in ethanol shows lower intensity PL emission than the colloid in water. In addition, in the Nd-based solutions in ethanol the second emission line was observed at around 1325 nm attributable to the $^4F_{3/2} \rightarrow {}^4I_{13/2}$ transition. This band is very weak and broad but is not observed in aqueous samples. Thus, the broad inhomogeneous luminescence band observed in the PL spectra of colloidal solutions in comparison with the initial solutions of neodymium nitrate indicates the doping of zinc oxide with neodymium. In addition, UV excitation of the luminescence of neodymium ions, which does not have absorption bands in this region, may indicate the transfer of excitation from zinc oxide matrix to Nd^{3+}, which additionally confirms the incorporation of Nd^{3+} into the ZnO lattice as a result of the synthesis.

Although the exact mechanism of excitation transfer from the ZnO host to the Nd^{3+} is unknown, we suggest based on the PL and PL excitation spectra (Figures 7, 9, and 10) that the energy transfer most probably occurs through the localized defect state within the ZnO band gap. After the band gap excitation of ZnO nanocrystals, the broad band PL in the visible region which is typical to the defect-containing zinc oxide nanostructures and NIR emission associated with the $^4F_{3/2} \rightarrow {}^4I_{11/2}$ transitions of Nd^{3+} ions were observed. The defect states are excited in result of the energy transfer following the recombination of electron–hole pair (exciton) formed upon the band gap excitation of ZnO. The defect states within the band gap of ZnO may further transfer energy non-radiatively to the $^4F_{3/2}$ level of neodymium ion with the subsequent emission in the range 1050–1080 nm. Similar energy transfer mechanisms were considered in the literature [37, 38, 39, 40].

Under the direct excitation at 580 and 800 nm, i.e. at the resonant lines of Nd^{3+} ion, the recorded luminescence spectra consist of two bands corresponding to the emission of Nd^{3+} ions with a dominant band at 1052–1057 nm and a band at around 1325 nm, which are related to radiative transitions from the $^4F_{3/2}$ level to the levels of the low-lying multiplet $^4I_{11/2}$ and $^4I_{13/2}$, respectively (Figures 10 (c-d)). It is

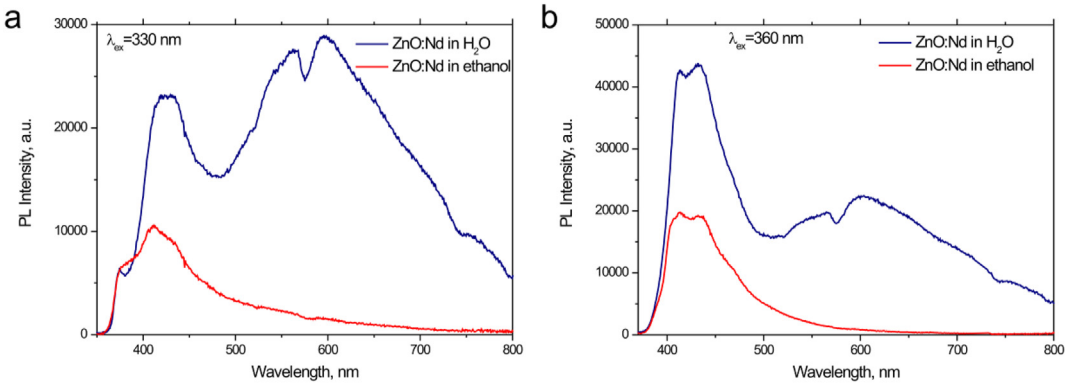

Figure 9. Photoluminescence spectra of the colloids prepared by laser ablation of zinc in $Nd(NO_3)_3$ solutions in water and ethanol registered in the visible region under 330 nm (a) and 360 nm (b) excitation.

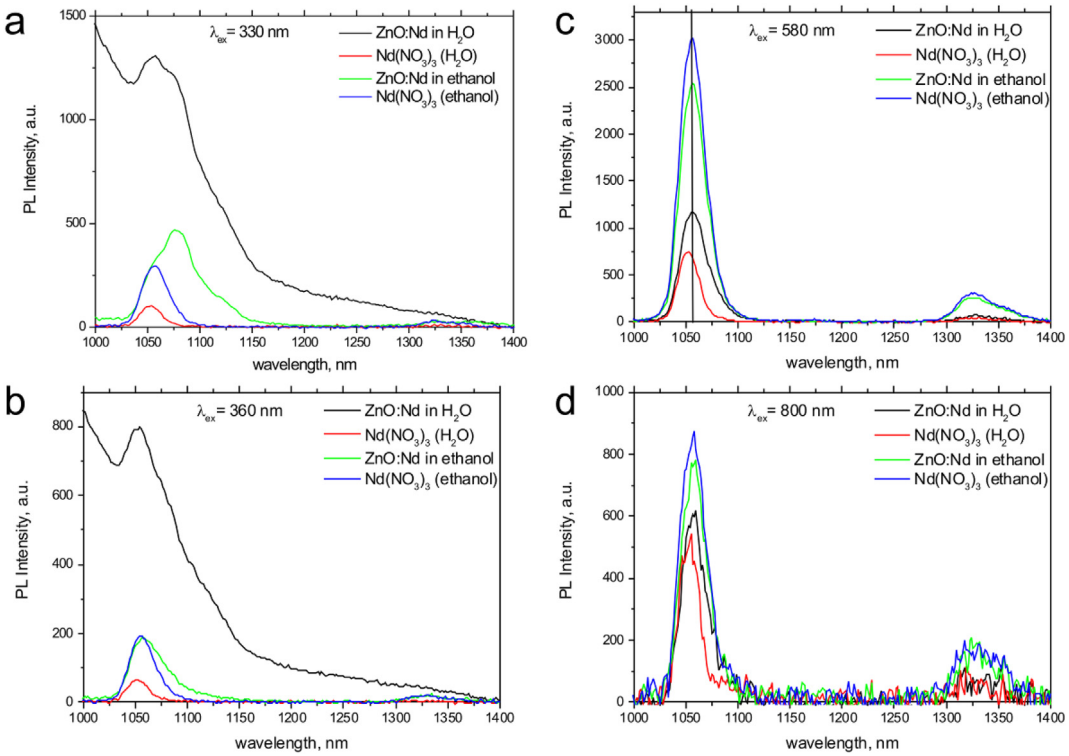

Figure 10. NIR PL emission spectra of the colloids obtained by laser ablation of Zn in $Nd(NO_3)_3$ aqueous and ethanol solutions at different excitation wavelengths: 330 nm (a), 360 nm (b), 580 nm (c), 800 nm (d). The PL spectra of the initial $Nd(NO_3)_3$ solutions in water and ethanol are shown for comparison.

noteworthy that under both 580 and 800 nm excitation wavelengths the NIR PL peaks position differed from those observed under the indirect UV excitation The difference in NIR luminescence spectra under indirect and direct excitation can be a result of the influence of crystal field environment on the Nd^{3+} energy levels positions, that may serve as an additional confirmation of the Nd^{3+} introduction into the ZnO matrix [38].

It should be noted that the position of the $^4F_{3/2} \rightarrow {}^4I_{11/2}$ peak in the aqueous ZnO:Nd sample differs from their position in the solution of neodymium nitrate salt. Also in the case of ZnO:Nd colloids, the positions and shapes of the bands in recorded luminescence spectra differ from Nd_2O_3 NPs spectra provided in the literature [41], which gives the additional evidence of the Nd^{3+} inclusion into ZnO nanocrystals.

Thus, laser ablation of a zinc target in a neodymium nitrate solution allows fabricating zinc oxide nanocrystals doped with Nd^{3+}. As indicated above, the interest to this kind of nanostructures is related to their potential application for biovisualization of tissues, since they have a number of suitable excitation and emission bands in the biological transparency windows and are characterized by low toxicity and long-term luminescence independent of the particle size.

As an example, the luminescence spectra of the obtained colloids recorded under 800 nm-excitation (Figure 10d) at room temperature exhibit characteristic emission bands of Nd^{3+} ions centered at about 1060 and 1334 nm. Our experiments showed that luminescence of these bands can be effectively excited by laser diodes with an emission wavelength close to 800 nm, where the absorption of water is minimal, these results serve as a prerequisite for the further biomedical application of the prepared ZnO nanocrystals doped with neodymium ions as luminescent biomarkers.

4. Conclusion

To conclude, the method of laser ablation in combination with laser-induced modification can be used to prepare ZnO nanocrystals doped with Nd^{3+} ions with NIR luminescence characteristic to the Nd^{3+} ions. The formation of neodymium-doped ZnO nanocrystals of a hexagonal

wurtzite structure with a particle average size in the range 1–10 nm was confirmed by the TEM and X-ray diffraction measurements.

It has been found that the efficient way to incorporate neodymium ions into the ZnO nanocrystals is to use the laser ablation method in an aqueous solution of a neodymium salt, that is confirmed by the observation of the IR luminescence of the Nd^{3+} ions in the prepared samples. The characteristic NIR luminescence of Nd^{3+} ions upon UV excitation indicates the transfer of excitation energy from the zinc oxide matrix to neodymium ion that proves the formation of neodymium-doped zinc oxide NPs. It was found that upon synthesis in both aqueous and ethanol solutions, the luminescence band of Nd^{3+} in the range 1054–1079 nm has a wide inhomogeneous profile, which indicates the formation of emission centers of different origin. Additional laser irradiation of the formed colloid allows increasing the emission intensity and improving the crystallinity of the formed NPs by their laser-induced heating.

The results of the optical properties study confirm that a liquid medium can serve as a tool for control over the characteristics of ZnO:Nd NPs obtained by laser ablation in a liquid. The preparation of NPs in an aqueous solution allows obtaining higher concentrations of particles than in ethanol, as evidenced by a more intense absorption band of ZnO. In addition, the experiments showed that the method of laser ablation in an aqueous solution allows obtaining particles with a higher NIR-luminescence intensity than in the case of synthesis in an ethanol solution. On the other hand, the intensity of defect luminescence in the visible region is also higher in the aqueous colloids than in alcoholic ones.

Declarations

Author contribution statement

Natalie Tarasenka: Conceived and designed the experiments; Performed the experiments; Analyzed and interpreted; Wrote the paper.

Vladislav Kornev: Performed the experiments; Contributed reagents, materials, analysis tools or data.

Andrei Ramanenka: Analyzed and interpreted the data; Contributed reagents, materials, analysis tools or data.

Ruibin Li: Conceived and designed the experiments; Analyzed and interpreted the data.

Nikolai Tarasenko: Conceived and designed the experiments; Analyzed and interpreted the data; Wrote the paper.

Funding statement

This work was supported by the National Academy of Sciences of Belarus (Convergence 2.2.05) and by the Belarusian Republican Foundation for Fundamental Research (F 20KITG-008 and F 21KOR-006).

Data availability statement

Data will be made available on request.

Declaration of interests statement

The authors declare no conflict of interest.

Additional information

No additional information is available for this paper.

References

[1] B. del Rosal, U. Rocha, E.C. Ximendes, E. Martín Rodríguez, D. Jaque, J. García Sole, Nd^{3+} ions in nanomedicine: perspectives and applications, Opt. Mater. 63 (2016) 185–196.

[2] D. Daksh, Y. Kumar Agrawal, Rare earth-doped zinc oxide nanostructures: a review, Rev. Nanosci. Nanotechnol. 5 (2016) 1–27.

[3] V. Kumar, O.M. Ntwaeaborwa, T. Soga, V. Dutta, H.C. Swart, Rare earth doped zinc oxide nanophosphor powder: a future material for solid state lighting and solar cells, ACS Photonics 4 (2017) 2613–2637.

[4] S. Kumar, P.D. Sahare, Nd-doped ZnO as a multifunctional nanomaterial, J. Rare Earths 30 (2012) 761.

[5] Hongli Du, Victor Castaing, Dongcai Guo, Bruno Viana, Rare-earths doped-nanoparticles prepared by pulsed laser ablation in liquids, Ceram. Int. 46 (2020) 26299–26308.

[6] D. Zhang, B. Gökce, S. Barcikowski, Laser synthesis and processing of colloids: fundamentals and applications, Chem. Rev. 117 (2017) 3990–4103.

[7] N. Tarasenka, A. Butsen, V. Pankov, T. Velusamy, D. Mariotti, N. Tarasenko, Laser assisted preparation of doped ZnO nanocrystals, Nano-Struct. Nano-Objects 12 (2017) 210–219.

[8] G.W. Yang, Laser ablation in liquids: applications in the synthesis of nanocrystals, Prog. Mater. Sci. 52 (2007) 648–698.

[9] S.A. Kulinich, T. Kondo, Y. Shimizu, T. Ito, Pressure effect on ZnO nanoparticles prepared via laser ablation in water, J. Appl. Phys. 113 (2013), 033509.

[10] N.N. Tarasenka, V.V. Pankov, A.V. Butsen, N.V. Tarasenko, Laser assisted synthesis, structural and magnetical characterization of gadolinium germano-silicide nanoparticles in liquid, J. Nanosci. Nanotechnol. 16 (2016) 7451–7460.

[11] M. Honda, T. Goto, T. Owashi, A.G. Rozhin, S. Yamaguchi, T. Ito, S.A. Kulinich, ZnO nanorods prepared via ablation of Zn with millisecond laser in liquid media, Phys. Chem. Chem. Phys. 18 (2016) 23628–23637.

[12] T. Chitradevi, A.J. Lenus, N.V. Jaya, Structure, morphology and luminescence properties of sol-gel method synthesized pure and Ag-doped ZnO nanoparticles, Mater. Res. Express 7 (2020), 015011.

[13] M. Carofiglio, S. Barui, V. Cauda, M. Laurenti, Doped zinc oxide nanoparticles: synthesis, characterization and potential use in nanomedicine, Appl. Sci. 10 (2020) 5194.

[14] E. Gorohova, L. Basyrova, I. Venevtsev, I. Alekseeva, A. Khubetsov, O. Dymshits, M. Baranov, M. Tsenter, A. Zhilin, S. Eron'ko, E. Oreschenko, P. Rodnyi, P. Loiko, Structure and spectral-luminescent properties of Er^{3+}:ZnO optical ceramics, J. Phys. Conf. 1695 (2020), 012041.

[15] A. El Fakir, M. Sekkati, A. Belayachi, Z. Edfouf, M. Regragui, F. Cherkaoui El Moursli, M. Abd-Lefdil, Influence of rare earth (Nd and Tb) Co-doping on ZnO thin films properties, Phys. Status Solidi C (1-4) (2017) 1700169.

[16] Y. Liu, W. Luo, R. Li, H. Zhu, X. Chen, Near-infrared luminescence of Nd^{3+} and Tm^{3+} ions doped ZnO nanocrystals, Opt Express 17 (2009) 9748–9753.

[17] D. Chen, F. Zhang, L. Lv, Z. Han, Y. Wang, Y. Gu, H. Chen, Bovine serum albumin coated upconversion nanoparticles for near infrared fluorescence imaging in mouse model, J. Nanosci. Nanotechnol. 17 (2017) 932–938.

[18] O. Yayapao, T. Thongtem, A. Phuruangrat, S. Thongtem, S. Thongtem, Ultrasonic-assisted synthesis of Nd-doped ZnO for photocatalysis, Mater. Lett. 90 (2013) 83–86.

[19] J. Zhang, S.J. Deng, S.Y. Liu, J.M. Chen, B.Q. Han, Y. Wang, Y.D. Wang, Preparation and photocatalytic activity of Nd doped ZnO nanoparticles, Mater. Technol. 29 (2014) 262–268.

[20] J. de Boor, T. Dasgupta, U. Saparamadu, E. Müller, Z. Ren, Recent progress in p-type thermoelectric magnesium silicide based solid solutions, Mater, Today Energy 4 (2017) 105–121.

[21] N.V. Tarasenko, A.V. Butsen, Laser synthesis and modification of composite nanoparticles in liquids, Quant. Electron. 40 (2010) 986–1003.

[22] H. Mateos, R.A. Picca, A. Mallardi, M. Dell'Aglio, A. De Giacomo, N. Cioffi, G. Palazzo, Effect of the surface chemical composition and of added metal cation concentration on the stability of metal nanoparticles synthesized by pulsed laser ablation in water, Appl. Sci. 10 (2020) 4169.

[23] J. Zhang, J. Claverie, M. Chaker, D. Ma, Colloidal metal nanoparticles prepared by laser ablation and their applications, ChemPhysChem 18 (2017) 986–1006.

[24] V. Merk, C. Rehbock, F. Becker, U. Hagemann, H. Nienhaus, S. Barcikowski, In situ non-DLVO stabilization of surfactant-free, plasmonic gold nanoparticles: effect of Hofmeister's anions, Langmuir 30 (2014) 4213–4222.

[25] J.Z. Marinho, L.F. de Paula, E. Longo, A.O.T. Patrocinio, R.C. Lima, Effect of Gd^{3+} doping on structural and photocatalytic properties of ZnO obtained by facile microwave-hydrothermal method, SN Appl. Sci. 1 (2019) 359.

[26] P. Rauwel, A. Galeckas, E. Rauwel, Enhancing the UV emission in ZnO–cnt hybrid nanostructures via the surface plasmon resonance of Ag nanoparticles, Nanomaterials 11 (2021) 452.

[27] L.M. Moreira, V. Anjos, M.J.V. Bell, C.A.R. Ramos, L.R.P. Kassab, D.J.L. Doualan, P. Camy, R. Moncorge, The effects of Nd_2O_3 concentration in the laser emission of TeO_2-ZnO glasses, Opt. Mater. 58 (2016) 84–88.

[28] S. Rakpanich, P. Meejitpaisan, S. Ravangvong, J. Kaewkhao, Effect of Nd^{3+} ion on bismuth borosilicate glass properties, Key Eng. Mater. 702 (2016) 13–17.

[29] A. Samanta, M.N. Goswami, P.K. Mahapatra, Influence of Nd^{3+} doping in ZnO nanoparticles to enhance the optical and photocatalytic activity, Mater. Res. Express 6 (2019), 065031.

[30] B. Lin, Z. Fu, Y. Jia, Green luminescent center in undoped zinc oxide films deposited on silicon substrates, Appl. Phys. Lett. 79 (2001) 943–945.

[31] H. Zeng, W. Cai, Y. Li, J. Hu, P. Liu, Composition/structural evolution and optical properties of ZnO/Zn nanoparticles by laser ablation in liquid media, J. Phys. Chem. B 109 (2005) 18260–18266.

[32] M. Willander, O. Nur, J.R. Sadaf, M.I. Qadir, S. Zaman, A. Zainelabdin, N. Bano, I. Hussain, Luminescence from Zinc Oxide nanostructures and polymers and their hybrid devices, Materials 3 (2010) 2643–2667.

[33] L.E. Greene, M. Law, J. Goldberger, F. Kim, J. Johnson, Y. Zhang, R.J. Saykally, P. Yang, Low temperature wafer-scale production of ZnO nanowires arrays, Angew. Chem. Int. Ed. 42 (2003) 3031–3034.

[34] M. Gomi, N. Oohira, K. Ozaki, M. Koyano, Photoluminescence and structural properties of precipitated ZnO fine particles, Jpn. J. Appl. Phys. 42 (2003) 481–485.
[35] A.B. Djurisic, Y.H. Leung, K.H. Tam, Y.F. Hsu, L. Ding, W.K. Ge, C. Zhong, K.S. Wong, W.K. Chan, H.L. Tam, K.W. Cheah, W.M. Kwok, D.L. Phillips, Defect emissions in ZnO nanostructures, Nanotechnology 18 (2007), 095702.
[36] P.P. Pal, J. Manam, Enhanced luminescenceof ZnO:RE^{3+} (RE=Eu, Tb) nanorods by Li^{+} doping and calculations of kinetic parameters, J. Lumin. 145 (2014) 340–350.
[37] M. Balestrieri, S. Colis, M. Gallart, Efficient energy transfer from ZnO to Nd^{3+} ions in Nd-doped ZnO films deposited by magnetron reactive sputtering, J. Mater. Chem. C 2 (2014) 9182–9188.
[38] Y. Liu, W. Luo, R. Li, X. Chen, Optical properties of Nd^{3+} ion-doped ZnO nanocrystals, J. Nanosci. Nanotechnol. 10 (2010) 1871–1876.
[39] S. Acosta, L.J. Borrero-González, P. Umek, L.A.O. Nunes, P. Guttmann, C. Bittencourt, Nd^{3+}-Doped TiO_2 nanoparticles as nanothermometer: high sensitivity in temperature evaluation inside biological windows, Sensors 21 (2021), 5306.
[40] E. Le Boulbar, E. Millon, E. Ntsoenzok, B. Hakim, W. Seiler, C. Boulmer-Leborgne, J. Perrière, UV to NIR photon conversion in Nd-doped rutile and anatase titanium dioxide films for silicon solar cell application, Opt. Mater. 34 (2012) 1419–1425.
[41] R.B. Yu, K.H. Yu, W. Wei, X.X. Xu, X.M. Qiu, S.Y. Liu, W. Huang, G. Tang, H. Ford, B. Peng, Nd_2O_3 nanoparticles modified with a silane-coupling agent as a liquid laser medium, Adv. Mater. 19 (2007) 838–842.